

PAPER • OPEN ACCESS

Additively manufactured Ti6Al4V lattice structures: mechanical characterization and numerical investigation

To cite this article: G Scalet *et al* 2021 *IOP Conf. Ser.: Mater. Sci. Eng.* **1038** 012057

View the [article online](#) for updates and enhancements.

Additively manufactured Ti6Al4V lattice structures: mechanical characterization and numerical investigation

G Scalet^{1,2*}, CA Biffi³, J Fiocchi³, A Tuissi³, F Auricchio^{1,2}

¹Department of Civil Engineering and Architecture, University of Pavia, Via Ferrata 3, 27100 Pavia, Italy

²Consorzio Interuniversitario Nazionale per la Scienza e Tecnologia dei Materiali (INSTM), Unità di Ricerca Pavia, Via Ferrata 3, 27100 Pavia, Italy

³National Research Council, Institute of Condensed Matter Chemistry and Technologies for Energy Unit of Lecco, CNR ICMATE, Via Previati 1/E, 23900 Lecco, Italy

*Corresponding author: giulia.scalet@unipv.it

Abstract. The interest in manufacturing complex devices with integrated extra-functional properties is steadily growing for high technological application fields, such as the aerospace and biomedical ones. Among advanced methods of manufacturing, additive manufacturing allows to produce complex three-dimensional geometries, like lattice structures, which possess mechanical and functional properties unachievable by their constituent materials. The present work investigates Ti6Al4V lattice structures produced by Selective Laser Melting (SLM) through a combined experimental and numerical campaign. The effects of the relative density of the elementary cell, building direction (along horizontal and vertical building directions), and sample condition (as-built and heat treated at 850°C) on the mechanical properties of the lattice structures are investigated through tensile testing. Finite element analysis is performed to analyze the stress/strain distribution due to the different investigated effects. The results provide useful insight into the deformation/failure mechanisms, stress concentrations, and mechanical properties of the studied structures as well as into their correlation to the relative density and printing process parameters. The resulting performances of the lattice structures are compared with the ones of the bulk samples.

1. Introduction

Lattice structures are three-dimensional open-cell architectures consisting of one or more repeating unit cells. These structures are characterized by a controlled relative density, defined by the ratio of the apparent density of the cellular structure to the density of the cellular structure's base material. Accordingly, such relative density depends on the dimensions and connectivity of the strut elements which constitute the unit cells and are connected at specific nodes [1]. Thanks to their geometry, lattice structures possess mechanical and functional properties unachievable by their base materials, such as high specific strength, lightweight, and shock absorption, that make them ideal candidates for medical [2], automotive [3], aeronautical [4], and seismic [5] applications.

Particularly, lattice structures made of metallic alloys are widely investigated in literature, being mainly oriented to biomedical devices in which low weight, low equivalent Young's moduli, and high osteointegration responses are highly demanded [6-7]. Moreover, metallic lattice structures are



Content from this work may be used under the terms of the [Creative Commons Attribution 3.0 licence](https://creativecommons.org/licenses/by/3.0/). Any further distribution of this work must maintain attribution to the author(s) and the title of the work, journal citation and DOI.

promising for enhancing the damping behavior for the suppression of mechanical vibrations and as acoustic insulators, heat exchangers, and, generally, light structures with high capability of deformation [8].

The huge commercial usefulness of metallic lattice structures as well as the continuing advancements on Additive Manufacturing (AM) technologies, in which the layer-by-layer building strategy offers designers the greatest possible freedom [9], motivate research efforts to propose reliable design approaches and characterization methods for a comprehensive understanding of the mechanical and functional properties of such structures [10]. In this regard, main challenges are associated to the fact that the mechanical and functional properties of these structures are significantly affected by different factors as unit cell's topology and relative density, boundary and loading conditions, heat treatment, and fabrication process parameters [10].

Among metallic AM technologies, the most diffused ones are electron beam melting [11-16] and selective laser melting [17-21], based on local melting of metallic powders deposited in a uniform bed by high power electron or laser beams, respectively.

Particularly, Ti6Al4V and CoCr alloys have been deeply investigated for realizing lattice and cellular structures mainly for biomedical applications, while the interest about 316L and AlSi10Mg alloys is growing in the prospective of mechanical and aerospace applications. In these cases, the compression and fatigue behavior of trabecular structures and the influence of process parameters, thermal treatments, and geometric features on the mechanical performances have been studied [18, 20, 22-29]. Moreover, different geometries and materials have been adopted and optimized in order to meet specific needs. For example, trabecular structures were proven instrumental in lowering the elastic modulus of Ti alloys down to about 1 GPa, so as to match the rigidity of bones and avoid dangerous stress shielding effect in biomedical implants [17]. Aluminum lattice structures with graded density were optimized in order to act as efficient energy absorbing material (up to 6,3 MJ/m³) in low-weight structures [30]. Moreover, it was found that process parameters, such as powder morphology and size, scanning strategy, power, scan speed, build direction, and layer thickness, affect the strength, modulus, microstructure, as well as dimensional accuracy of lattice structures (see [10, 26] and references therein).

On the contrary, the damping response as well as the tensile behaviour of lattice structures remain an area requiring further research. In dynamic applications, in fact, trabecular structures possess damping performances significantly higher than the fully dense ones, making them ideal materials for energy absorption [26, 31-33]. Moreover, mechanical testing under compression is generally preferred due to the easier setup compared to testing under tension [34].

To avoid the costs of fabrication and experimentation of metallic lattice structures, the formulation of models is highly desirable for accurately predicting their structural behavior and for allowing efficient numerical design simulations at acceptable computational expenses. To date, finite element models of either the entire lattices or single unit cells [6, 21-22, 25, 35-36] as well as homogenization approaches [37] represent the most used tool for predicting the behavior of these structures. Such models allow to analyze material behavior dependence on loading conditions, lattice topology, cell relative density, and presence of imperfections or defects as well as to obtain design maps [38]. Alternative approaches for reducing computational expense, but often at the cost of accuracy, e.g., beam-based models or Gibson-Ashby models, have been proposed (see [10] and references therein). Topology optimization is often used for designing lattice structures satisfying the requirements of different applications [39-40].

Motivated by the discussed framework, the present work aims to investigate the effect of the relative density of the elementary cell on the mechanical material properties of a lattice structure fabricated by AM.

An experimental investigation is first performed on Ti6Al4V lattice structures and full density dogbone shaped samples, produced by Selective Laser Melting (SLM), which is the most diffused technology among AM. Thereafter, two elementary cells, representative of two values of relative density, are considered and realized as lattice samples. In particular, due to the limited data on tensile performances of these structures, static mechanical behaviour in tension is studied by taking into account the two principal manufacturing orientations (i.e., parallel and orthogonal to the building platform) as

well as material treatment condition (i.e., as-built and heat treated at 850°C for two hours). Then, a numerical finite element analysis is performed to analyze the effect of the elementary cell on stress/strain distribution, in order to ease the description and discussion of the experimental results.

The obtained results allow to provide useful insight into the deformation/failure mechanisms, stress concentrations, and mechanical properties of the studied structures as well as into their correlation to the relative density and printing process parameters. A discussion on the calibration of the material parameters employed in the numerical model is further provided.

The paper is organized as follows. Section 2 describes the material and the adopted methodology. Then, Section 3 presents and discusses the results of the experimental and numerical investigation. Finally, conclusions are given in Section 4.

2. Materials and methods

2.1. Material and manufacturing

Spherical gas atomized Ti6Al4V powder, whose chemical composition is reported in Table 1, was used. The powder featured a particles size between 20 μm and 63 μm with average size of approximately 45 μm .

Table 1: Chemical composition of the TiAl6V4 powder (wt. %).

Al	V	Fe	O	C	N	H	Ti
6	4	< 0.25	< 0.13	< 0.08	< 0.05	< 0.012	bal.

Two types of lattice samples were produced by means of a SLM system (mod. AM400 from Renishaw), equipped with a pulsed wave fiber laser. Both lattice structures were based on a tetragonal diamond-like structure; the structures, indicated as L18.5 and L22.1, had 18.5% and 22.1% of relative density with respect to full dense parts. Strut diameter was 1 mm, while strut length was 2.5 mm and 1.23 mm for L18.5 and L22.1, respectively. The lattice samples were manufactured with prismatic geometry (10 mm \times 10 mm \times 30 mm in size) and oriented in the xy and xz directions (i.e., respectively, along horizontal and vertical building directions), as depicted in Figure 1. Standard process parameters, suggested by Renishaw, are listed in Table 2. The used laser scanning strategy was concentric, as usually adopted for thin and lattice structures. Each scanning layer was rotated by 67° with respect to the previous one, and the scheme was repeated every 180 layers. During the SLM process, the O₂ content was below 100 ppm.

The samples were tested in the as-built (AB) condition and after heat treatment (HT), performed in vacuum at 850 °C for two hours and hereafter rapidly cooled in flowing argon atmosphere, according to the indications from the material's datasheet [41].

As reference, fully dense dogbone samples, according with the standard [42], were manufactured with the same process parameters used for the printing of the lattice structures and were used for the identification of the material constitutive model employed in the numerical simulations (see Section 2.3).

Table 2: SLM process parameters used for manufacturing the lattice samples.

Parameter	Value
Power	100 W
Exposure time	60 μs
Point distance	75 μm
Hatch distance	75 μm
Hatch offset	60 μm
Layer thickness	30 μm

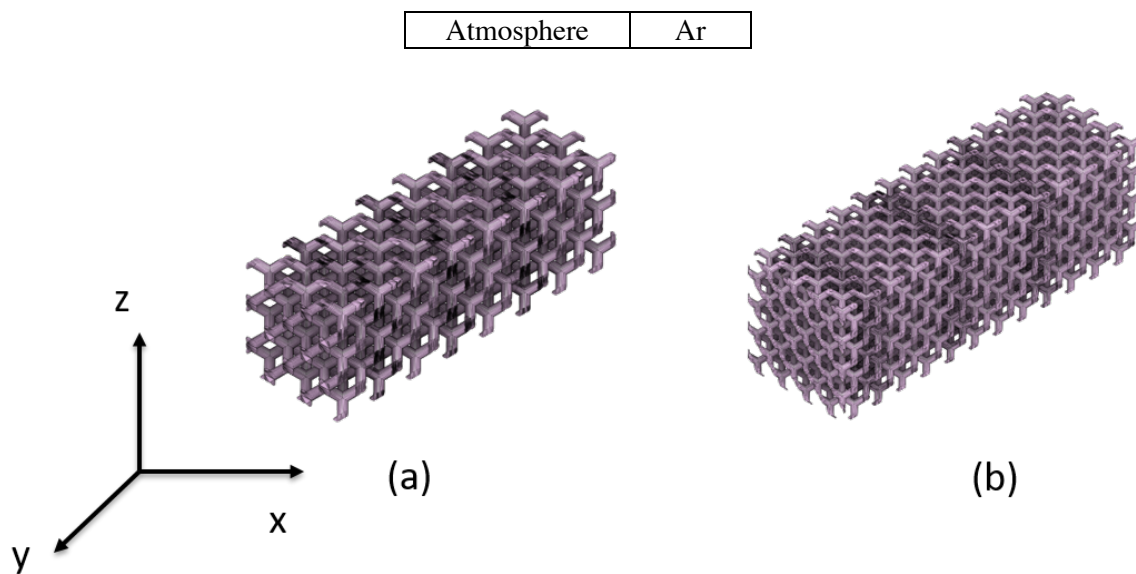


Figure 1: Schematic of the lattice structure manufactured in TiAl6V4 having relative density of (a) 18.5% and (b) 22.1%, respectively.

2.2. Mechanical characterization

Quasi-static mechanical properties were evaluated by means of an MTS 2/M machine (strain rate of 0.015 min^{-1}). Tensile testing was performed on full dense dogbone specimens and on the lattice structures. Three samples for each manufacturing condition (i.e. without and with homogenization heat treatment) and printing direction were tested. All samples were tested along their main axes (lying either in the xy or xz planes) and up to complete failure. In order to calculate engineering stress and strain of lattice structures, the nominal section and length of the whole structure itself were considered, as if it were a dense part [43]. This allowed to better highlight the change in mechanical properties with respect to the bulk samples.

2.3. Numerical simulations

To predict and analyze the results of the quasi-static mechanical characterization, finite element analyses (FEA) were performed using the commercial finite element software Abaqus (Simulia, Providence, RI, USA).

The two lattice geometries reported in Figure 1 were meshed using four-node tetrahedral elements (C3D4), available in the software library. The mesh of the L18.5 structure was defined by 21898 nodes and 65401 elements, while the mesh of the L22.1 structure by 136771 nodes and 419979 elements.

Since the lattice structures were made of Ti6Al4V alloy and the analyses had to simulate monotonic behavior, a J2 elastoplastic constitutive model with isotropic hardening was adopted. The constitutive model is already implemented within the software material library and its parameters were identified on tensile stress-strain curves obtained from full dense dogbone specimens.

To simulate the mechanical characterization on lattice structures under uniaxial tensile loads, a quasi-static analysis was performed under large displacements. A displacement was applied along the main axis direction on the upper face of the structure, while classical boundary conditions were applied on the other faces.

3. Results and discussion

3.1. Mechanical Characterization

Tensile tests were performed on fully dense dogbone specimens, built along xy and xz directions, in the AB and HT conditions. Figure 2 shows the stress-strain curves of the Ti6Al4V dogbone samples, while Table 3 lists the main tensile characteristics, i.e. Young’s modulus, yield and ultimate stress, and elongation to fracture.

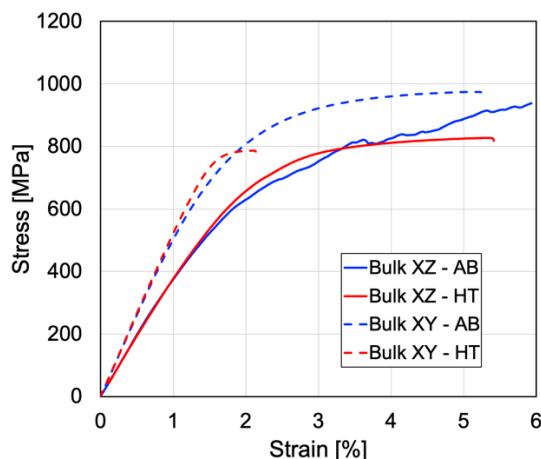


Figure 2: Tensile stress-strain curves of the Ti6Al4V full dense dogbone specimens under different conditions and printing orientations.

Table 3: Elastic modulus (E), yield stress (YS), ultimate tensile stress (UTS) and elongation to failure (ϵ) of the Ti6Al4V full dense dogbone samples tested under tensile conditions.

Samples			E (GPa)	YS (MPa)	UTS (MPa)	ϵ (%)
Geometry	Building direction	Condition				
Bulk	xy	AB	40.6	726.3	974.2	5.3
		HT	41.7	763.1	833.9	4.4
	xz	AB	38.4	542.3	938.3	5.9
		HT	39.4	621.6	826.9	5.4

Then, tensile tests were performed on both lattice structures, built along xy and xz directions, in the AB and HT conditions. Figures 3(a) and 3(b) show the experimental tensile stress-strain curves for the lattice structure L18.5 and L22.1, respectively.

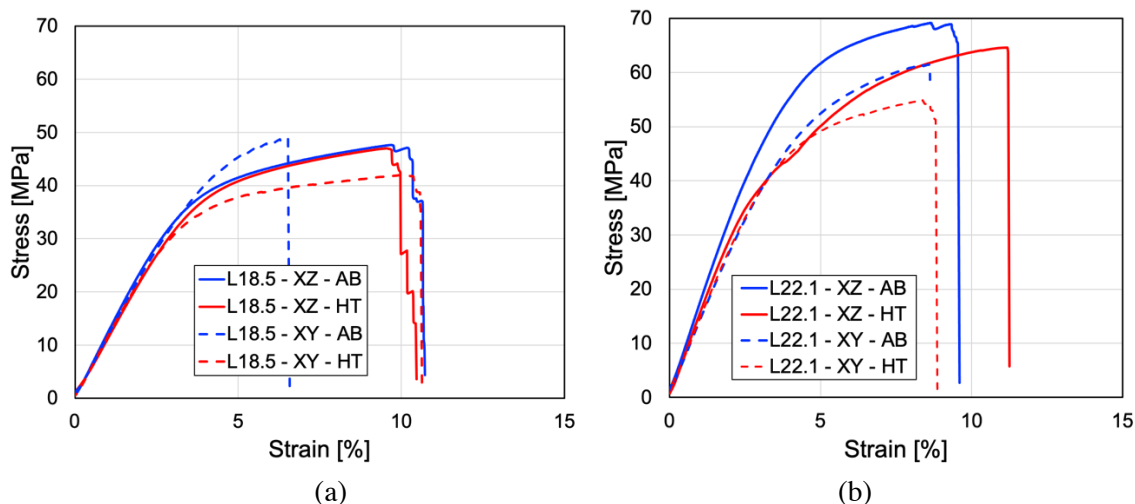


Figure 3: Tensile stress-strain curves of the Ti6Al4V lattice structures with relative density of (a) 18.5% and (b) 22.1%, respectively, under different treatment conditions and printing orientations.

All curves show a linear elastic behavior up to yielding, followed by plastic deformation up to failure.

It may be appreciated that, as expected, the trabecular structures are characterized by much lower stiffness and mechanical resistance than corresponding bulk samples and that, accordingly, higher elastic moduli characterize L22.1 with respect to L18.5 trabecular samples. Thus, according to literature results [6], the mechanical properties decrease with reduced relative density. On the contrary, elongation to failure is largely higher in trabecular samples than in bulk parts.

Mechanical behavior of the considered lattice samples was only slightly affected by building direction per se. Minor differences in elastic modulus values of samples built along different directions should probably be ascribed to measurement variability. This is reasonable, since the orientation of the struts is the same between vertical and horizontal samples.

However, production strategy did have a strong influence on the effect of heat treatment. As far as parts built on the xy plane are concerned, heat treated samples show a distinct decrease in ultimate tensile stress with respect to as-built ones. The reduction amounts to approximately 18% and 1% for bulk and trabecular samples, respectively. On the other hand, this difference is much smaller for samples built in vertical direction and approaches zero in the case of trabecular specimens. The present trend may be ascribed to the well-known problem concerning the build-up of residual stresses during the selective laser melting process. According to [44], residual stresses in as-built Ti6Al4V parts can be as high as 265 MPa along x direction and they are completely cancelled by heat treatment at temperatures equal or higher than 800 °C. It is reasonable to suppose that residual stresses are higher in samples, which during production were attached to the building plate through a larger area, hence the difference in mechanical behavior induced by heat treatment is more marked for specimens built on xy plane. Moreover, bulk samples are likely more affected by residual stresses because of their higher mass.

Final failure of samples happened abruptly in bulk samples, whereas it happened by progressive breaking of single struts in trabecular structures. As evident in Figure 4, in trabecular structures failure took place by shearing due to progressive breakage of struts along a plane lying at 45° with respect to stress direction, which is in agreement with what is reported in literature for compression tests [18, 24]. On the other hand, bulk samples failed along less geometrically defined planes, reasonably because of their limited thickness. At higher magnification all fracture surfaces revealed a mixed ductile-brittle behaviour. Although small dimples, induced by relevant plastic deformation, were prevalent across all fracture surfaces, some cleavage-like planes, frequently localized at defects (lack of fusion defects or round gas porosities) could also be found.

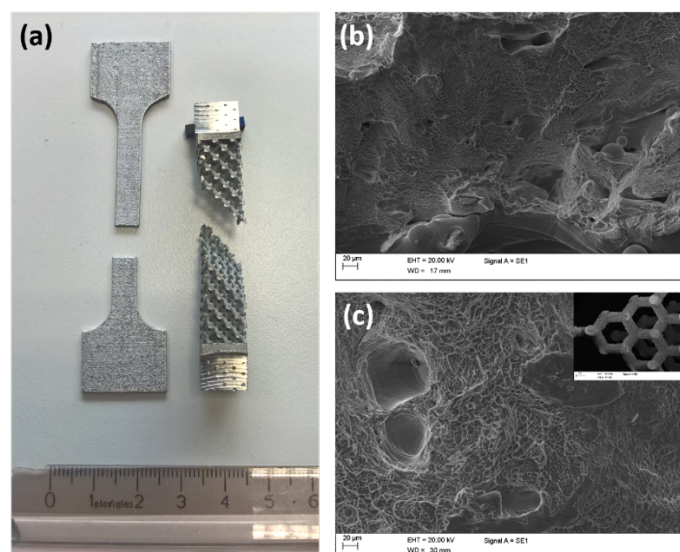


Figure 4: (a) Macroscopic appearance of broken tensile samples; magnification of fracture surfaces of (b) bulk and (c) lattice samples.

3.2. Numerical simulations

Numerical simulations were performed to predict the tensile behavior of the two lattice structures (see Figure 3). Accordingly, the parameters of the J2 elastoplastic constitutive model with isotropic hardening were calibrated on the four stress-strain curves reported in Figure 2. This way, four sets of model parameters were obtained for each condition (i.e., XY-AB, XY-HT, XZ-AB, and XZ-HT) and were used to predict the corresponding lattice structures' behaviour.

Figures 5(a) and 5(b) show the experimental and predicted tensile stress-strain curves for the lattice structure L18.5, respectively in the AB and HT condition, while Figures 5(c) and 5(d) show the experimental and predicted tensile stress-strain curves for the lattice structure L22.1, respectively in the AB and HT condition. In general, good agreement between numerical and experimental curves can be observed for most of the cases. In fact, consistently with experimental data, numerical results predict the decrease of the mechanical properties with decreasing relative density. Moreover, the model shows higher strength of the as-built structures than the heat treated ones.

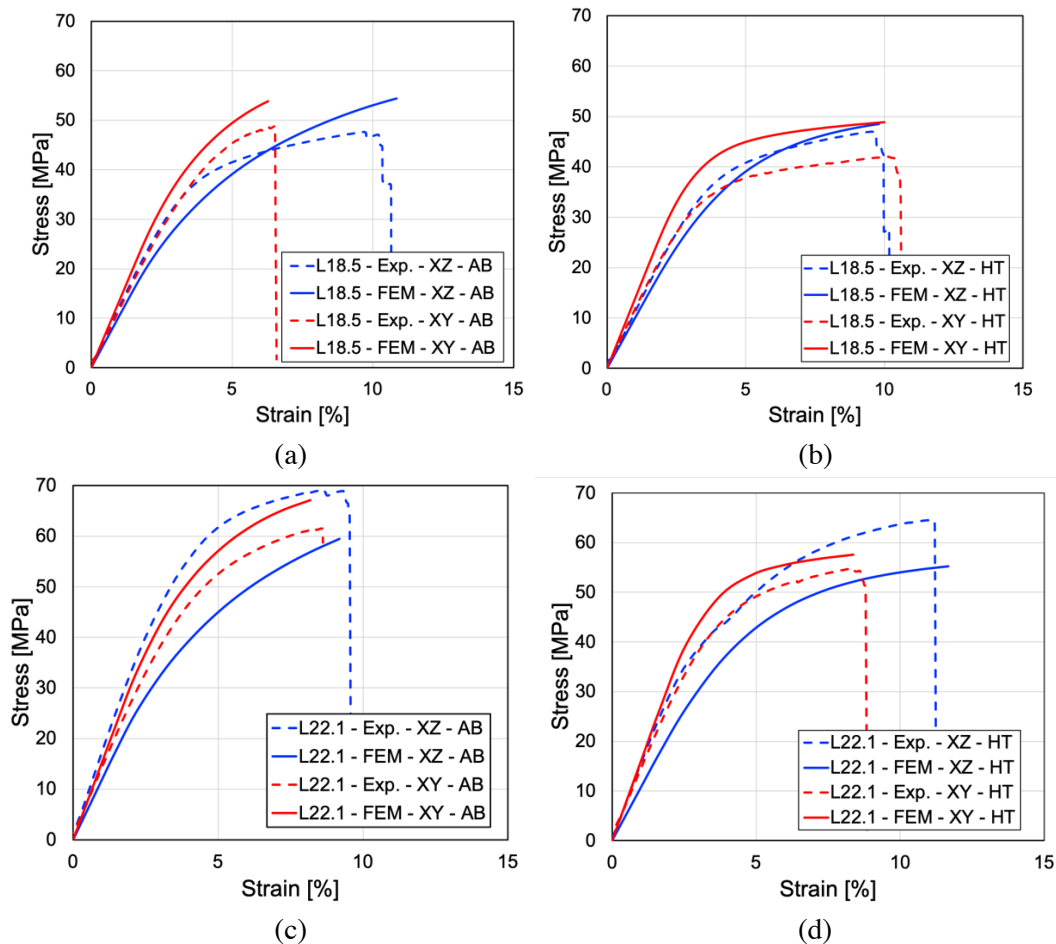


Figure 5: Tensile stress-strain curves of the Ti6Al4V lattice structure with relative density of 18.5% in the (a) AB and (b) HT condition and different printing directions, respectively, and of the lattice structure with relative density of 22.1% in the (c) AB and (d) HT condition and different printing directions, respectively.

To quantify the goodness of numerical results, Table 4 reports the relative errors on the computation of the elastic modulus and yield stress from experimental and finite element curves reported in Figure 5. Relative errors vary between a minimum value of 1.7% and a maximum value of 33.3%. Major differences between experimental and numerical results are evident for the lattice structure L22.1 built along the xz direction. It must be recognized that the experimental mechanical behaviour of this particular sample appears to be definitely out of trend with respect to other samples. Therefore, this discrepancy between experimental and numerical description of the L22.1 sample shall likely be ascribed to experimental variability rather than to a defectiveness of the model. Moreover, the discrepancy may be due to some variations between the finite element model and the produced lattice structures. In fact, the manufactured lattice may have defects, caused by the SLM process, which can affect the overall mechanical behaviour, as well as residual stresses causing anisotropic material behaviour. Moreover, it should be highlighted that the adopted constitutive model is very simple and does not take into account anisotropic and tension-compression asymmetric material behavior.

Table 4: Relative errors on the elastic modulus (e_E) and yield stress (e_{YS}) of the lattice samples tested under tensile conditions between experimental and numerical results.

Samples			e_E (%)	e_{YS} (%)
Geometry	Building direction	Condition		
Lattice L18.5	xy	AB	13.9	12.4
		HT	24.3	24.4
	xz	AB	6.4	18.5
		HT	10.6	14.7
Lattice L22.1	xy	AB	15.4	8.0
		HT	18.8	1.7
	xz	AB	27.5	33.3
		HT	28.4	15.0

Finally, in order to provide insight about stress and strain distribution along the lattice structures, the contour plot of the von-Mises equivalent stress (MISES) is reported, respectively, in Figure 6 and 7 for the two trabecular structures under tensile load. As it can be noted, both lattice structures are characterized by high values of the von-Mises equivalent stress in the as-built condition. As expected from the predicted stress-strain curves, the structures printed along the xy direction show higher values compared to the xz direction. Stress concentrations are present close to the intersection of diagonal struts.

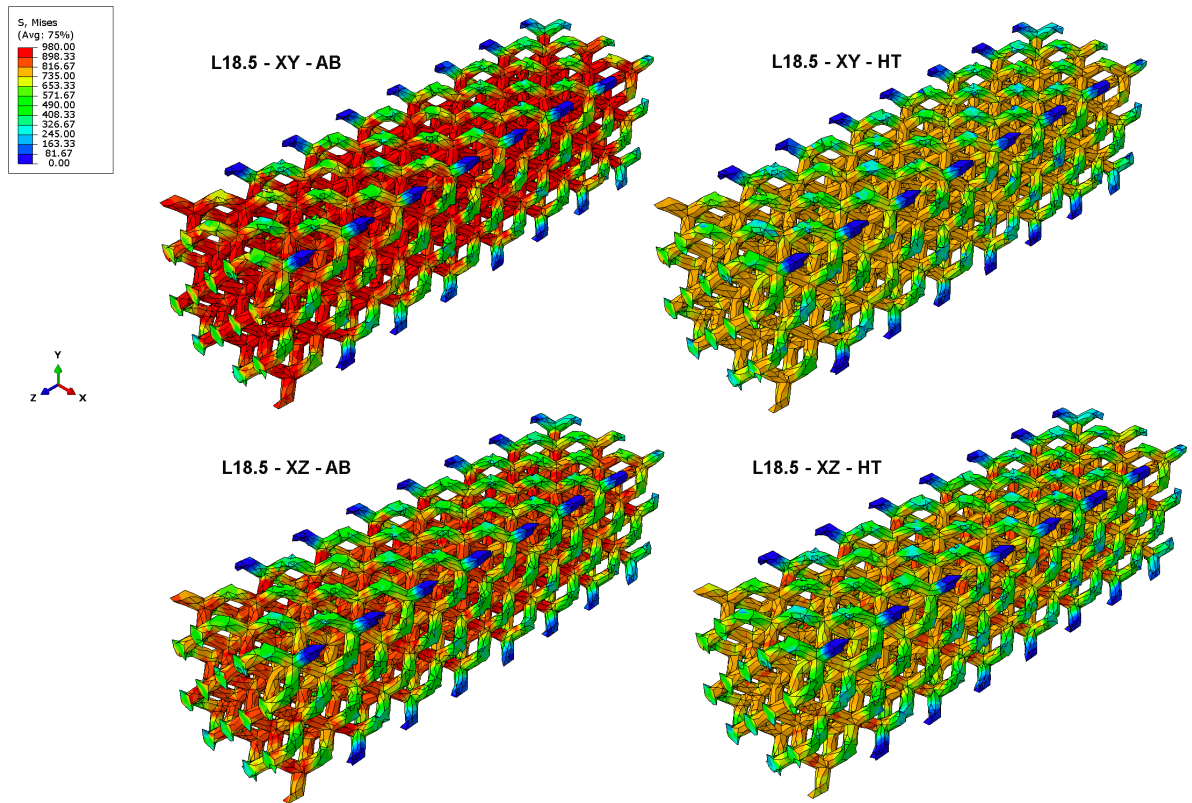


Figure 6: Contour plot of the von-Mises equivalent stresses (MISES) [MPa] for the trabecular structure with relative density of 18.5% under tensile load.

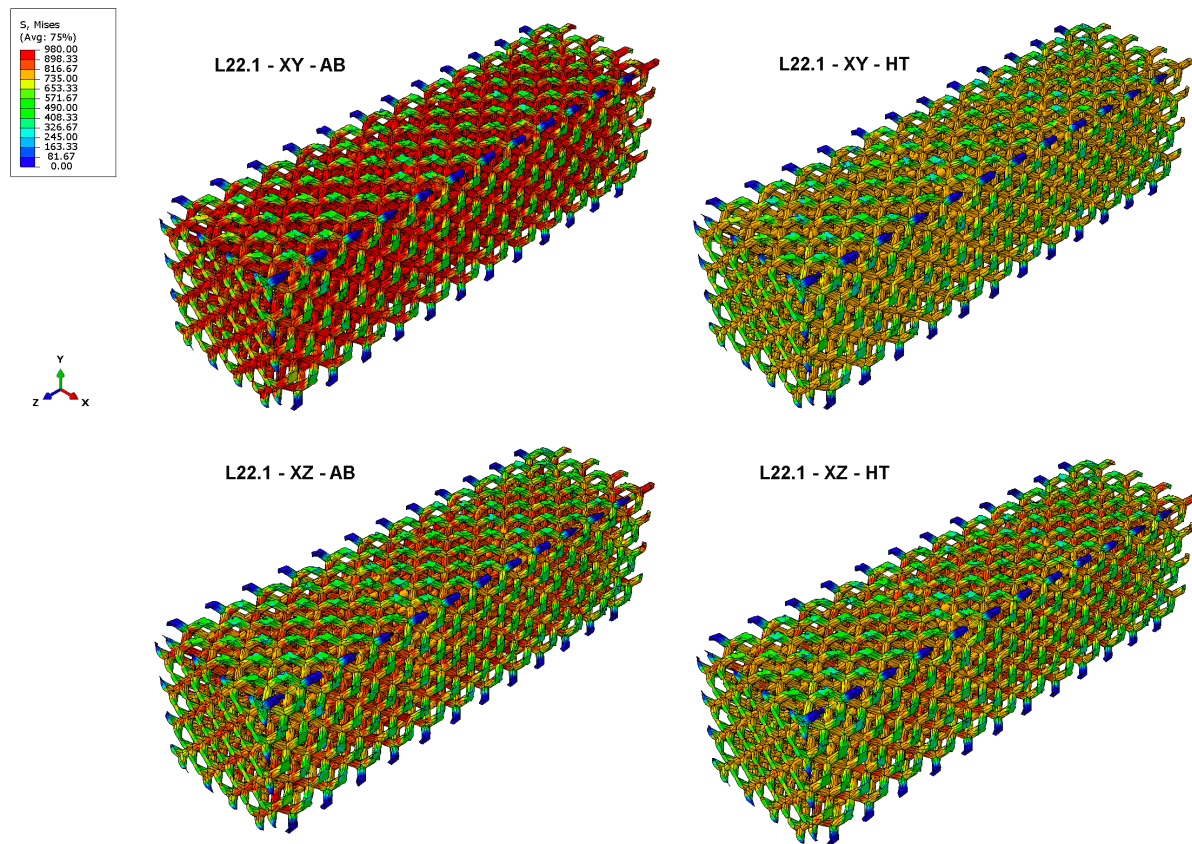


Figure 7: Contour plot of the von-Mises equivalent stresses (MISES) [MPa] for the trabecular structure with relative density of 22.1% under tensile load.

The contour plot of the equivalent plastic strain (PEEQ) is reported, respectively, in Figure 8 and 9 for the two trabecular structures under tensile load. The results show that plastic strain is higher for the structures subjected to heat treatment.

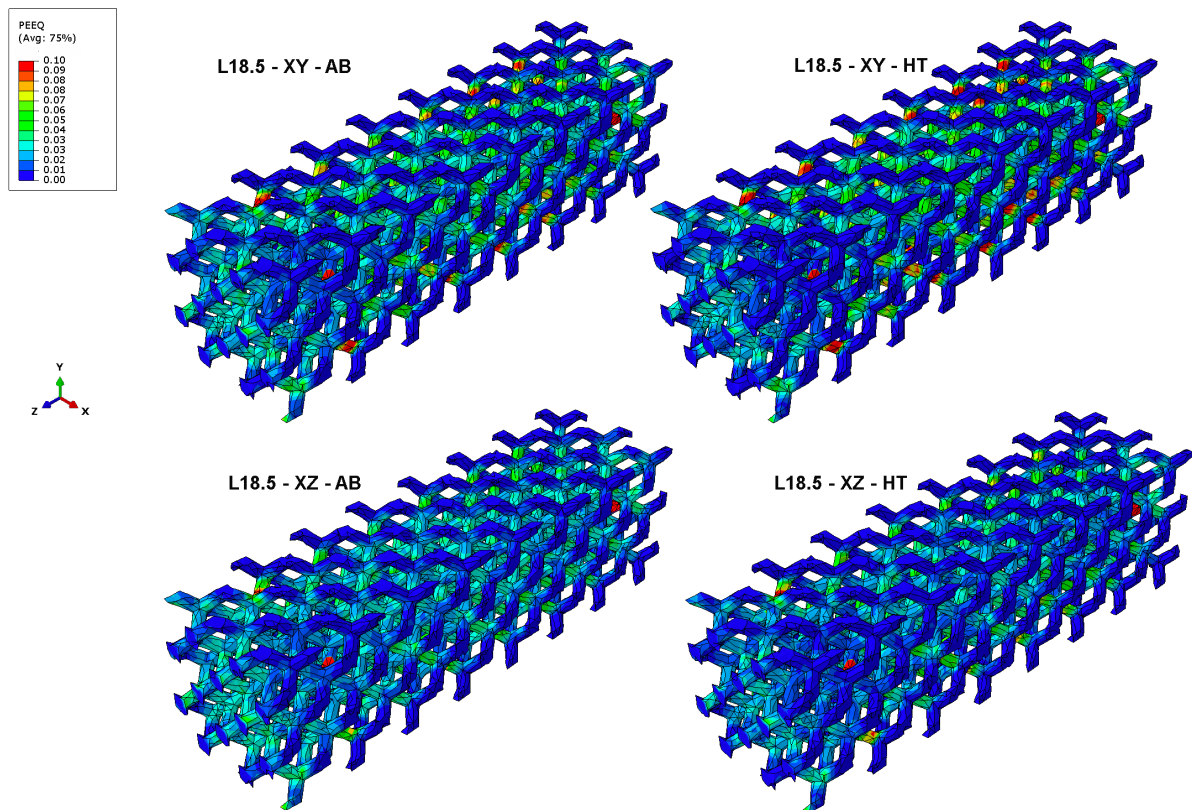


Figure 8: Contour plot of the equivalent plastic strain (PEEQ) [-] for the trabecular structure with relative density of 18.5% under tensile load.

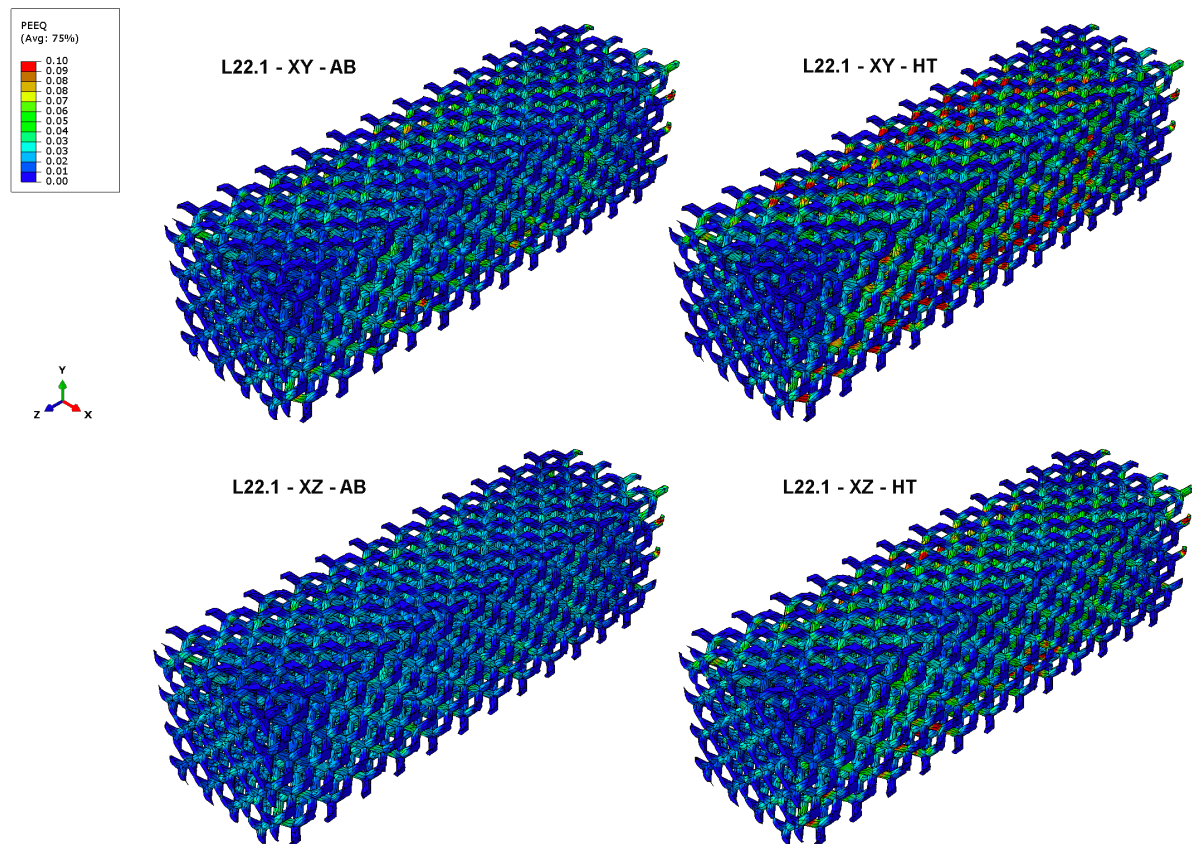


Figure 9: Contour plot of the equivalent plastic strain (PEEQ) [-] for the trabecular structure with relative density of 22.1% under tensile load.

4. Conclusions

This paper has presented an experimental and numerical investigation of the tensile behavior of lattice structures having two different relative densities. The design of lattice structures has been successful in giving rise to structures with low, and tunable, stiffness and ductility higher than the bulk material. The effect of both printing direction and heat treatment has been investigated and the behavior of lattice structures has been compared to the results on bulk specimens. Experimental and numerical results predict an overall consistent behavior. The observed discrepancies may be associated to the manufacturing process: the real manufactured structures may be, in fact, different from the ideal ones simulated through finite element analysis. A simple constitutive J_2 elastoplastic model has been adopted and calibrated on data from bulk specimens realized with the same procedure applied to the lattice structures. Such an identification process of model parameters is fundamental for obtaining coherent results, given the variability of 3D printed material response. However, more complex constitutive material behavior could be also adopted. Finally, it should be highlighted that tensile testing results should be considered with caution, since many different effects concurred to determine the final result. In particular, the mechanical behaviour may not be perfectly approximated to the one of standard dog-bone samples. As a matter of fact, different features, including scanning strategy, thickness, inclination and distance from the building plate, may alter the microstructure of real lattice struts, thus possibly yielding unexpected behaviours.

Acknowledgements

This work was partially supported by the Italian Minister of University and Research through the project "A BRIDGE TO THE FUTURE: Computational methods, innovative applications, experimental validations of new materials and technologies" (No. 2017L7X3CS) within the PRIN 2017 program, by Regione Lombardia through the project "MADE4LO - Metal ADditivE for LOmbardy" (No. 240963) within the POR FESR 2014-2020 program, by the project "Nuovi materiali e approcci computazionali per stampa 4D" of INSTM Consortium, and by Accordo Quadro CNR/Regione Lombardia n. 3866 of 17/07/2015 FHfFC. The authors would like to acknowledge Nicola Bennato and Giordano Carcano from CNR-ICMATE for their assistance and support in the experiments.

References

- [1] Gibson L J and Ashby M F 1997 *Cellular Solids: Structure and Properties* (Cambridge University Press)
- [2] Egan P F, Gonella V C, Engelsperger M, Ferguson S J, Shea K 2017 *PLoS ONE* **12**(8) e0182902
- [3] Aslan B and Yildiz A R 2020 *Mater Test* **62**(6) 633-639
- [4] Vasiliev V V, Barynin V A, Razin A F 2012 *Compos Struct* **94**(3) 1117-1127
- [5] Kong D, Fan F, Zhi X 2014 *Int . Steel Struct* **14** 901-911
- [6] Burton H E, Eisenstein N M, Lawless B M, Jamshidi P, Segarra M A, Addison O, Shepherd D E T, Attallah M M, Grover L M, Cox S C 2019 *Mater Sci Eng C* **94**(1) 901-908
- [7] Obaton A F, Fain J, Djemaï M, Meinel D, Léonard F, Mahé E, Lécuelle B, Fouchet J J, Bruno G 2017 *Heliyon* **3** e00374
- [8] Ramadani R, Belsak A, Kegl M, Predan J, Pehan S 2018 *Int J Simul Model* **17**(1) 92-104
- [9] Nagesha B K, Dhinakaran V, Varsha Shree M, Manoj Kumar K P, Chalawadi D, Sathish T 2020 *Mater Today Proc* **21**(1) 916-919
- [10] Maconachie T, Leary M, Lozanovski B, Zhang X, Qian M, Faruque O, Brandt M 2019 *Mater Des* **183** 108137
- [11] Parthasarathy J, Starly B, Raman S, Christensen A 2010 *J Mech Behav Biomed Mater* **3** 249-259
- [12] Cheng X Y, Li S J, Murr L E, Zhang Z B, Hao Y L, Yang R, Medina F, Wicker R B 2012 *J Mech Behav Biomed Mater* **16** 153-162
- [13] Li S J, Murr L E, Cheng X Y, Zhang Z B, Hao Y L, Yang R, Medina F, Wicker R B 2012 *Acta Mater* **60** 793-802
- [14] Murr L E, Gaytan S M, Medina F, Martinez E, Martinez J L, Hernandez D H, Machado B I, Ramirez D A, Wicker R B 2010 *Mater Sci Eng A* **527**: 1861-1868
- [15] Marin E, Lanzutti A, Turchet S, Fusi S, Pressacco M, Fedrizzi L 2011 *La Metallurgia Italiana* **103** 27-36
- [16] Biffi C A, Fiocchi J, Ferrario E, Fornaci A, Riccio M, Romeo M, Tuissi A 2020 *Int J Adv Manuf Technol* 1-12
- [17] Chen W M, Xie Y M, Imbalzano G, Shen J, Xu S, Lee S J, Lee P V S 2016 *Int J Prec Eng Manufact* **17** 793-799
- [18] Crupi V, Kara E, Epasto G, Guglielmino E, Aykul H 2017 *Mater Des* **135** 246-256
- [19] Sallica-Leva E, Jardini A L, Fogagnolo J B 2013 *J Mech Behav Biomed Mater* **26** 98-108
- [20] Choy S Y, Sun C N, Leong K F, Wei J 2017 *Addit Manuf* **16** 213-224
- [21] Leary M, Mazur M, Elambasseril J, McMillan M, Chirent T, Sun Y, Qian M, Easton M, Brandt M 2016 *Mater Des* **98** 344-357
- [22] Zhong T, He K, Li H, Yang L 2019 *Mater Des* **181** 108076
- [23] Campanelli S L, Contuzzi N, Ludovico A D, Caiazzo F, Cardaropoli F, Sergi V 2014 *Mater (Basel)* **7** 4803-4822
- [24] Wauthle R, Vrancken B, Beynaerts B, Jorissen K, Schrooten J, Kruth J P, Van Humbeeck J 2015 *Addit Manuf* **5** 77-84
- [25] Plessis A, Yadroitsava I, Yadroitsev I 2018 *Opt Laser Technol* **108**: 521-528
- [26] Sing S L, Wiria F E, Yeong W Y 2018 *Robot Com-Int Manuf* **49** 170-180
- [27] Feng Q, Tang Q, Liu Y, Setchi R, Soe S, Ma S, Bai L 2018 *Int J Adv Manuf Tech* **94** 2301-2313

- [28] Fatemi A, Molaei R, Sharifimehr S, Phan N, Shamsaei N 2017 *Int J Fatigue* **100** 347-366
- [29] Hanks B, Berthel J, Frecker M, Simpson T W 2020 *Addit Manuf* **35** 101301
- [30] Maskery I, Aboulkhair N T, Aremu A O, Tuck C J, Ashcroft I A, Wildman R D, Hague R J M 2016 *Mater Sci Eng A* **670** 264-274
- [31] Gong L, Kyriakides S, Jang W Y 2005 *Int J Solids Struct* **42** 1355-1379
- [32] Deodati P, Donnini R, Montanari R, Testani C 2009 *Mater Sci Eng A* **522** 318-321
- [33] Fiocchi J, Biffi C A, Scaccabarozzi D, Saggin B, Tuissi, A 2020 *Adv Eng Mater* **22** 1900722
- [34] Alsalla H, Hao L, Smith C 2016 *Mater Sci Eng A* **669** 1e6
- [35] Rosa F, Manzoni S, Casati R 2018 *Mater Des* **160** 1010-1018
- [36] Zhou H, Zhao M, Ma Z, Zhang D Z, Fu G 2020 *Int J Mech Sci* **175** 105480
- [37] Peng C, Tran P, Nguyen-Xuan H, Ferreira A J M 2020 *Compos Struct* **235**(1) 111821
- [38] Qi D, Yu H, Liu M, Huang H, Xu S, Xi Y, Qi G, Wu W 2019 *Int J Mech Sci* **163** 105091
- [39] Xiao Z, Yang Y, Xiao R, Bai Y, Song C, Wang D 2018 *Mater Des* **143** 27-37
- [40] Wiedingn J, Wolf A, Bader R 2014 *J Mech Behav Biomed Mater* **37** 56-68
- [41] Renishaw plc, Ti6Al4V ELI-0406 powder for additive manufacturing, 2017.
- [42] ASTM standards, E8/E8M: standard test methods for tension testing of metallic materials, Annu. B. ASTM Stand. 4: 1-27, 2010. doi:10.1520/E0008.
- [43] Ashby M F, Evans T, Fleck N A, Hutchinson J W, Wadley H N G, Gibson L J 2000 *Metal foams: a design guide* (Elsevier)
- [44] Leuders S, Thöne M, Riemer A, Niendorf T, Tröster T, Richard H A, Maier H J 2013 *Int J Fatigue* **48** 300-307